

# THE DESIGN AND TESTING OF A SURFACE TENSION DRIVEN WATER PUMP

J Fraser<sup>a</sup> & RT Dobson<sup>b</sup>

Department of Mechanical Engineering, University of Stellenbosch, Cape Town, South Africa  
Private Bag X1, Matieland 7602, South Africa

Water pumping is essential for life as we know it. The drive for alternative energies together with the need for water pumping has inspired the construction of a surface tension driven water pump (STDWP). The goal of this study was to construct and test a passive water pump inspired by tree water transport mechanisms. Here various experimental tests were done to determine the STDWP's performance and behaviour under various environmental conditions and pumping heads. Theoretical mass transfer relations were used to model the evaporative rate from the "leaf" surface and compared to the experimentally measured results. It was found that the developed pump could pump water at a rate of nearly 400 mL/hr.m<sup>2</sup>, reaching pumping heads of 1.8 m, with a maximum functional lifespan of 13 days. The STDWP's water collection efficiency was found to be 98% on average. The mechanistic causes of pump failure are addressed with recommendations for the STDWP improvement.

**Introduction:** Water pumping is an important part of our daily lives as it allows access to water for nourishment, industrial processes, irrigation, etc. Over millions of years, nature has developed efficient ways to cope with the daily struggle for survival. Biomimicry tries to find creative, efficient and economical solutions to modern day problems by attempting to imitate structures and processes found in nature [1,2]. Examples include increased aerodynamics of bullet trains (kingfisher nose), extra lift and efficiency of wind turbine blades (whale fins), reduced water drag materials (shark skin), improved strength of lightweight structures (honeycombs) and many more [1]. Further, Koch and Barthlott [3] reveal some of the advantages of super hydrophobic and super hydrophilic plant surfaces as inspiration for biomimetic materials. The potential for super hydrophobic materials with self-cleaning qualities as well as significant drag reduction in water and for super hydrophilic materials with enhanced capillary liquid transport are explained.

In nature, trees and plants are able to draw water from deep underground through their roots and up to their leaves to be used in processes such as photosynthesis. Certain trees, such as Giant Redwoods, as seen in Figure 8, can grow exceptionally high, up to 100 m tall. Water is thus effectively pumped below ground level to this height. Consequently, the mechanisms employed in plant water transport would seem to be an energy-efficient and eco-friendly method for water transport. The initiative to develop "green"

technologies, with an emphasis on the reduction of carbon emissions, has inspired the development of an "artificial" tree or a tree inspired passive pump.

Research based on artificial trees is fairly limited to botanists e.g. Susman et al. [4] and Martinez Vilalta et al. [5], attempting to model the water transport mechanism in trees for lecturing purposes. Further vaguely related work includes transpiration-based micro-pumps with continuous ultra-low flow rates [6], microfluidic systems formed in synthetic hydrogel [7], electro-wetting for microfluidic transport [8], synthetic leaf charged-pumping [9], wireless solar water splitting in an artificial leaf [10] and artificial tree carbon absorption [11,12]. Bulk water transport systems inspired by water transport mechanisms in trees have not yet been developed. The study and development of such systems can possibly lead to future designs for eco-friendly processes in industry. Further applications for such a passive water pump, beyond the microfluidic scope, can include a stand-alone passive water pump for green buildings or poverty stricken communities in Africa and even efficient rooftop cooling by evaporation.

The mechanisms through which water transport in plants occur were studied together with surface tension, bubble nucleation theory, water under tension as well as general water properties. This study was then employed to aid in the development of passive/"artificial" tree-like water pump. The constructed passive water pump was then experimentally tested to ascertain its behaviour and general performance under various environmental conditions. A theoretical thermo-hydraulic simulation was also conducted and validated against the experimental results. A simplified statistical formulation was generated from the experimental data for simple predictions and was compared to the theoretical thermo-hydraulic simulation. In this study, a description of STDWP design with the materials used will be presented. Further, a summary of the experimental methodology with the desired outcomes are given. Finally a discussion of the results with some recommendations is reported.

**Theory:** In-depth research was done on various topics relating to water transport in trees. This was necessary as understanding plant structures and surface tension as well as phase change mechanisms will encourage the development of a successful design.

<sup>a</sup>E-mail: 15689859@sun.ac.za

<sup>b</sup>Tel: 27 808 4268; Fax: 27 808 4958; E-mail: rtd@sun.ac

**Surface Tension:** The surface tension phenomenon is very important, however, it frequently remains unnoticed and is regularly ignored. Surface tension results in a nearly elastic membrane-like surface at the interface between two fluids, which is able to deform slightly. Certain insects are able to support themselves on water surfaces [13] and some bacteria are able to propel themselves forward [14], all due to the effects of surface tension. Surface tension,  $\sigma$ , which arises between two or more bulk fluids can be explained by molecular interactions in the interfacial region. The interfacial region is a very thin region, most often a few molecules wide, between two bulk fluids where the fluid properties rapidly transforms from one bulk fluid to the other [15]. A liquid-vapour interface is shown in Figure 1 depicting the density variation across the interfacial region.

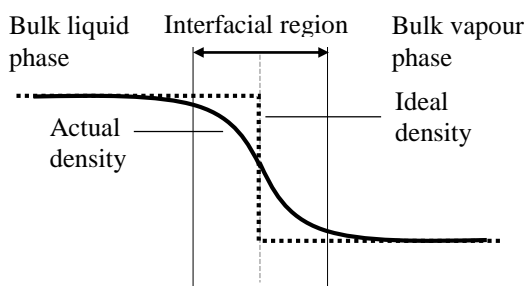


**Figure 1: Density distribution across liquid-vapour interface**

A Simplified representation of the attractive and repulsive nature of molecules with respect to their intermolecular distances can be explained when considering the Lenard-Jones intermolecular potential, shown in Figure 2. The Lenard-Jones model shows the greater sensitivity of close range repulsive forces to intermolecular distances as opposed to the longer range attractive forces.

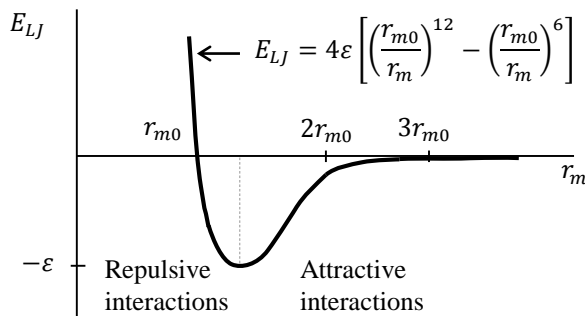


**Figure 2: Lenard-Jones intermolecular potential**

Considering a liquid which is in contact with its vapour phase, a molecule which is well within the liquid phase will be fully balanced and experience equal attractive as well as repulsive forces from all sides. However, at the interface, the molecular spacing is much less dense and therefore the repulsive forces decrease significantly with attractive forces only varying

slightly. Due to the weak molecular interactions experienced from the vapour phase, the attractive and repulsive forces perpendicular to the interface are balanced and very weak. Conversely, parallel to the interface the density distribution remains fairly uniform and therefore much stronger attractive intermolecular forces are experienced on either side of the molecule with weak repulsive intermolecular forces. A net tension which is equal in all directions and parallel to the interface (perpendicular to the density gradient) is induced among the molecules at the interface. Figure 3 presents a simplified force diagram of a molecule within the liquid phase and at the interface. The molecules at the interface are at an unfavourable energy state and therefore surface tension strives to minimise the interfacial area [15].

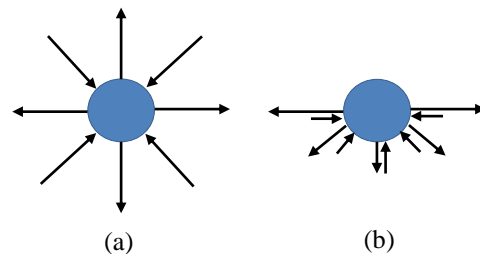


**Figure 3: Simple force diagram of a molecule (a) within the liquid phase and (b) at the liquid-vapour interface**

The total surface tension may be further subdivided into dispersion force ( $\sigma_d$ ) and hydrogen or metallic bond ( $\sigma_{h/m}$ ) contributions.

$$\sigma = \sigma_d + \sigma_{h/m} \quad (1)$$

Therefore, the reason why metallic liquids have much higher surface tensions than water or non-polar liquids can be explained, as metallic bonds are much stronger intermolecular interactions when compared to hydrogen bonds and dispersion forces. The above formulation indicates that the presence of either hydrogen bonds or metallic bonds will thus greatly increase the resulting surface tension [15].

Surface tension between two fluids may be affected through various mechanisms. Most commonly temperature and contaminants are used to alter surface tension. For a liquid in contact with its vapour phase the effect of temperature becomes intuitive. As the liquid is heated to a certain critical temperature, the two fluids will eventually tend to become identical at the interface and therefore the surface tension will decrease as temperature increases. For an increase in contaminant concentration, surface tension will generally decrease significantly. In this case, the contaminant is called a surfactant (surface active agent). A surfactant will accumulate at the interface and has a much lower surface tension than that of water [15]. The reason for increase of surfactant concentration at the interface is water's affinity to develop preferred hydrogen bonds. The water molecules will reconfigure such that the impurities are

forced to the interface and that the least amount of tetrahedral charges point to the most unaccommodating species [16].

The forces due to a liquid meniscus as a direct result of surface tension are called capillary forces. There are three equations primarily used to describe liquid interfaces [17]. Firstly, the Young-Laplace equation relates the interfacial curvature to the interfacial pressure drop. Secondly, the Kelvin equation relates the interfacial geometry to the liquid's vapour pressure. Finally, Young's equation relates the solid-liquid-vapour interaction and can be used to describe the wettability of a surface.

The Young-Laplace equation for small systems in equilibrium may be written as follows [15]

$$\Delta P = \sigma \left( \frac{1}{r_1} + \frac{1}{r_2} \right) \quad (2)$$

where  $\Delta P$  is the interfacial pressure drop and  $r_1$  and  $r_2$  relate to the interfacial radii of curvature. The Young-Laplace equation may be applied to a simple example such as a typical capillary tube (shown in Figure 4).

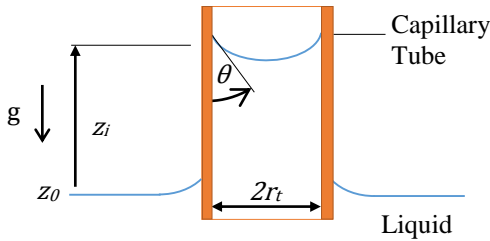


**Figure 4: Capillary tube**

For a capillary tube, as shown in Figure 4, with the assumption that the liquid surface is free and the liquid wets the tube surface ( $\theta < 90^\circ$ ), the equilibrium height,  $z_i$ , of the water column may be determined using Equation 3

$$z_i = \left[ \frac{2\sigma \cos(\theta)}{g(\rho_l - \rho_g)r_t} \right] \quad (3)$$

where  $g$  is the gravitational constant,  $\rho$  refers to density and  $\theta$  the contact angle. It can be seen that as  $r_t$  decreases  $z_i$  can become quite large. For a non-wetting case ( $\theta > 90^\circ$ ), the above equation would still be valid, but  $z_i$  will be negative. The Young-Laplace equation may be applied to describe much more complex geometries, such as sessile and pendant drops [15]

The Kelvin equation is derived from the Young-Laplace equation and the ideal gas law and can be expressed as [17]

$$R_{GC} T \ln \frac{P_v}{P_0} = \sigma \left( \frac{1}{r_1} + \frac{1}{r_2} \right) \quad (4)$$

where  $P_0$  is the saturation equilibrium vapour pressure (planar liquid surfaces,  $P_{sat}$ ),  $P_v$  is the subsequent vapour pressure,  $T$  is the temperature (in K) and  $R_{GC}$  is the specific gas constant.  $P_v$  can be used as an indication of how volatile a liquid is and its tendency

to evaporate. The Kelvin equation can once again be applied to a capillary tube, as in Figure 4, and it can be shown that

$$P_v = P_0 e^{\frac{-2\sigma \cos(\theta)}{TR_{GC}r_t}} \quad (5)$$

In the case of  $\theta < 90^\circ$  the resulting  $P_v$  will decrease, where for  $\theta = 90^\circ$  the resulting  $P_v$  remain the same and finally for  $\theta > 90^\circ$  the resulting  $P_v$  will increase. Therefore, a liquid with a meniscus as shown in Figure 4 will tend to evaporate less than the same liquid with a planar interfacial surface.

Young's equation for solid-liquid-vapour contact lines, as seen in Figure 5, can be written as follows

$$\sigma_{LV} \cos \theta = \sigma_{SV} - \sigma_{SL} \quad (6)$$

The three interfaces all contribute their own interfacial tension, that is,  $\sigma_{LV}$  (liquid-vapour),  $\sigma_{SL}$  (solid-liquid) and  $\sigma_{SV}$  (solid-vapour), where  $\sigma_{LV}$  is commonly known as  $\sigma$  (surface tension). Young's equation only applies to equilibrium conditions and does not account for pre-wetted surfaces, nor any adsorbed liquid films. The equation does indicate some interesting features and is primarily used to describe the wetting or non-wetting characteristics of a liquid on a surface. Although Young's equation is a rather simple formulation, it is difficult to apply in practice as little is known on solid-liquid and solid-vapour interfacial tensions [15].

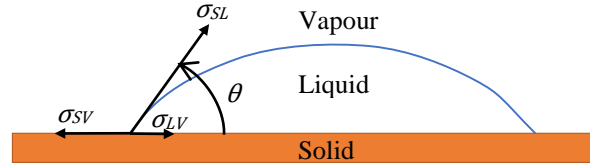


**Figure 5: Solid-liquid-vapour contact line**

*Metastable Water:* Water possesses some interesting and remarkable properties [18]. Due to the molecular structure of water, water molecules are able to attach to one another and bunch together which gives water strong cohesive properties. Furthermore, water molecules are easily attracted to polarized or charged surfaces which gives water its adhesive properties [19,18]. Experimentally, it has been observed that liquids can be heated above their theoretical saturation temperature without any phase transitions. In such cases, a liquid is said to be superheated and is in a non-equilibrium or metastable state [20]. The formation of vapour embryos which allow the growth of larger bubbles is called nucleation. The nucleation process may be homogenous (completely within the bulk fluid) or heterogeneous (at a solid-liquid interface), as shown in Figure 6 [20]. Water under tension is in a metastable state and has been studied for many years by various scientists. Classical theoretical estimates for the tensile strength of water ranges from 190 MPa to 230 MPa [21,19]. There, however, exists a large discrepancy between theoretical estimates and that of actual experimental results. The most reliable experiments consistently yield tensions closer to 30 MPa. Only in

quartz inclusions have tensions of 140 MPa ever been observed [21]. In most cases it is believed that the cause of phase change at higher tensions are heterogeneous and therefore a lack of adhesive forces rather than cohesive forces are responsible for the reported lower tensile strength values [22]. Sedgewick and Trevena [23] explore dynamic stressing of water as well as the boiling and/or deionization of water. Even lower tensile strengths of 1.4 MPa were reported for boiled and deionized water. It was determined that the boiling and/or deionization of water will increase the vaporisation threshold [23].

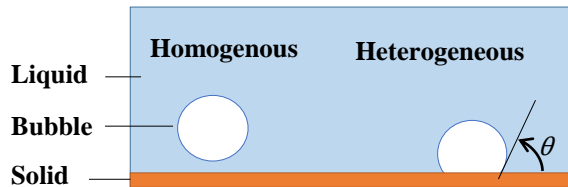


**Figure 6: Solid-liquid-vapour contact line**

*Basic Principles of Water and Solute Transport in Plants:* Most plant structures primarily focus on exposing a large surface area to the environment to enhance their exposure to sunlight and to increase the uptake of  $\text{CO}_2$  (from the air) and  $\text{H}_2\text{O}$  (from the ground) [24]. The cohesion-tension or transpiration-pull theory is the most widely accepted theory of water transport in plants. Here the strong cohesive and adhesive bonds of water molecules allow long continuous columns of water to exist within plant conduits (called xylem). Additionally, surface tension at the air-water interface in and between plant leaf cells (mesophyll cells) generate a large pressure difference which is able to sustain the water column height and flow rate. The flow rate is induced by the evaporation of water from the saturated leaf mesophyll cells into the intercellular air spaces which then diffuses to the environment through the leaf guard cells (stomata) [25]. The process of transpiration pull is shown in Figure 7. In Figure 7 it is shown that (1) water evaporates from thin film and forms menisci on the microfibrils of the primary cell walls as well as between the various leaf cells. (2) Water is then pulled from surrounding cells to replace the evaporative loss. The pull extends into the xylem, roots and soil. (3) Such that ground water enters the roots and is pulled into the xylem which transports the feed water to the leaf. In tall trees typical water tensions of 1.2 to 3.5 MPa have been reported with such highs as 17 MPa in certain plants [19].

Osmosis is the diffusion of water from a high water concentration to a low water concentration through a semipermeable membrane. In the roots of plants, there are many raw materials, nutrients and minerals which lowers the water concentration in the root with respect to the soil water concentration. A net (osmotic) pressure is induced due to the water concentration

gradient, called the root pressure, which pushes water from the root xylem into the stem xylem. The maximum height gained from typical root pressures is generally in the range of a few meters, which is far less than the height of a 100 m tall Giant Redwood (as seen in Figure 8). Root pressure has been found to be insignificant when compared to that of transpiration pull [25].

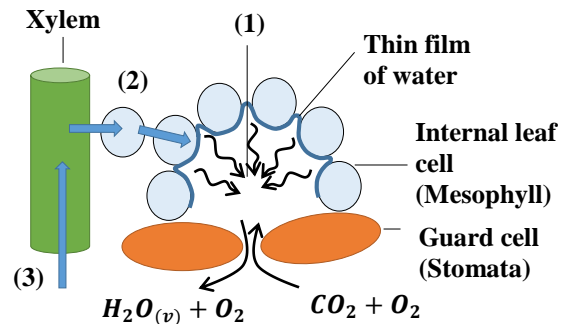


**Figure 7: Transpiration pull in leaf**

In tall trees a vacuum or even tension might be present in the xylem conduits. Therefore, the water in certain areas of the tree will be in a metastable state. The phase change of liquid water into vapour in these conduits is inevitable.



**Figure 8: Giant Redwood [26]**

Localised lower pressure regions will ultimately results in cavitation which leads to large bubble formation and finally an *embolism*. An embolism is the formation of a *critical* bubble size such that the water column in the xylem breaks. Such an event is ultimately unavoidable and therefore the plant vascular system consists of many clusters of xylem (tracheids and vessels) of various lengths [27]. Typical tracheid diameters and lengths range from 5 to 80  $\mu\text{m}$  and 0.1 to 1 cm, respectively. Vessels diameters and lengths vary between 15 to 500  $\mu\text{m}$  and 1 to 1000 (rare) cm, respectively [28]. Furthermore, xylem conduits possess pits which are intended to prevent air spreading from an air filled conduit into the transpiration stream. Various pit structures exist, where, most commonly, pit membranes and torus-margo structures are found in xylem conduits. The pit membrane consists of

uniformly distributed microfibrils with minute pore sizes ranging from 70 to 500 nm. The minute pores in the pit membrane are able to generate a strong enough meniscus to prevent air leaking into other water filled conduits. On the other hand, the torus-margo has a central thickened structure (torus) surrounded by a very porous structure (margo). When air is on one side of the torus-margo, the torus will be sucked in such that the margo is fully blocked and flow from the air filled conduit is stopped. Pit membranes present a very large flow resistance which is significantly reduced with the torus-margo adaptation. However, the torus-margo cannot restrict air leakages at very high pressure gradients [28]. Plants require CO<sub>2</sub> as well as water for cell tissue and photosynthesis. Therefore, plants must transpire to acquire both of these much needed molecules [27]. Various environmental conditions may act to enhance or even inhibit transpiration, as listed in Table 1.

**Table 1: Factors that affect transpiration [29]**

Factor	Description	Explanation
Light	Higher frequency light increases transpiration	The stomata opens wider to allow more carbon dioxide into the leaf for photosynthesis
Temperature	Higher temperatures causes an increase in transpiration	Higher temperatures increase evaporation and diffusion
Wind	Faster wind speed increases transpiration	Evaporation of water from the leaf is increased due to forced flow over the leaf surface (forced convection)
Humidity	Higher humidity conditions slows down transpiration	As the air is nearing saturation the amount of evaporation must decrease

Excessive transpiration will increase the stress in water filled conduits and might lead to the formation of embolisms. Therefore, it is imperative that there is a mechanism which can regulate the transpiration rate. In plants, the stomata inflates and deflates in an attempt to regulate the net plant water loss [27].

**Design layout:** Artificial trees have been constructed before by botanists such as Susman et al. [4] and Martinez Vilalta et al. [5], to demonstrate the water pumping ability of plants. The artificial “leaf” proposed here, however, is geared at demonstrating the

water pumping potential for such a passive pump and not to physically simulate plant transpiration mechanisms. Figure 9 shows a simplified schematic of the developed “leaf”. The “leaf” consists of an upper (1) and lower disc (2). Both discs were constructed from marine grade aluminium (AL 5083) for its relatively lightweight, strong and corrosion resistant properties. 12 M8 bolts (3) and nuts (4) were used to ensure that the two discs are firmly held together. A double set of O-rings (5) was used to prevent air entering the system from the outer edges. The upper disc features two brass needle valves. The primary needle valve (6) regulates feed water to the “leaf” while the secondary needle valve (7) is used to alleviate pressure buildup during the initial filling procedure as well as air and bubble removal from the “leaf”. Additionally, the upper disc contains a small chamber which houses the internal “leaf” materials. A set of 63  $\varnothing$ 7 mm holes (8), at varying PCD’s up to 80 mm were laser cut into the lower disc, as shown in Figure 10. The laser cut holes would provide openings for water vapour to escape from the “leaf” whilst keeping enough material to support the internal “leaf” material. A gasket (9) was placed on the lower disc to prevent air seepage past the internal “leaf” material through minute crevices in the discs.

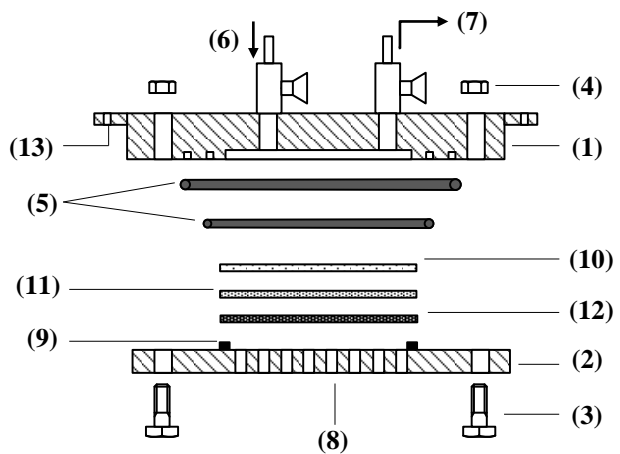


**Figure 9: STDWP “leaf” layout**

The internal “leaf” material consists of three layers: A super absorbent sponge material (10), made of high density PVA (polyvinyl alcohol) was used as the first layer. The PVA sponge was used as it is hydrophilic with estimated effective capillaries of 200  $\mu$ m which would help prevent bubble formation in the “leaf”. Thereafter,  $\varnothing$ 90 mm Grade 393 (Quantative) Munktell filter paper (11), with 1 to 2  $\mu$ m pores, was used as the second layer. The second layer is also hydrophilic and also helps prevent bubble formation in the “leaf”. Additionally, the second layer has much finer pores than the first layer which traps larger particles before reaching the final layer to prevent clogging of the final layer.

For the final layer Millipore membrane filters (12) were used. Both  $\varnothing$ 90 mm MF-Millipore™ membrane

filters (0.22  $\mu\text{m}$  pores, 3.52 bar bubble pressure) [30] as well as  $\text{Ø}90$  mm Durapore® (0.22  $\mu\text{m}$  pores, 3.45 bar bubble pressure) [31] were tested. MF-Millipore™ was found to work much more effectively than the Durapore® for this application. Scanning Electron Microscope (SEM) images were taken of the various internal “leaf” materials, as seen in Figure 11.



Figure 10: Lower “leaf” disc

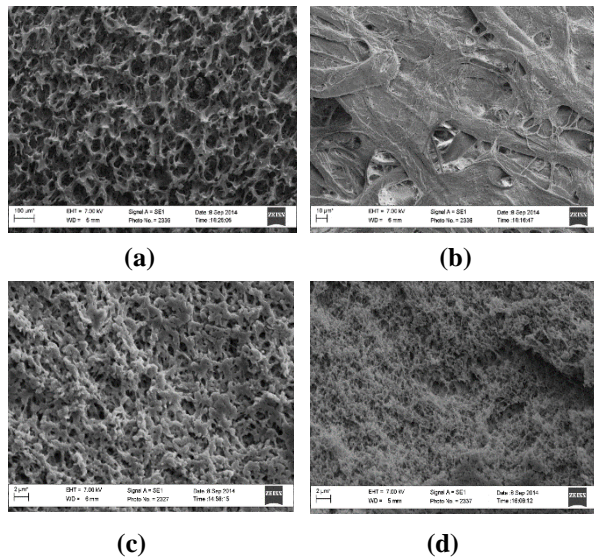


Figure 11: SEM images of internal “leaf” materials: (a) PVA sponge 200x magnification, (b) Munktell filter paper 1000x magnification, (c) Durapore® 7000x magnification and (d) MF-Millipore™ 7000x magnification

A flow diagram for a single branch system consisting of a single “leaf” is shown in Figure 12. The setup is relatively simple with  $\text{Ø}8$  mm (thick walled transparent) PVC hosing used to connect the “leaf” to the water source. A single larger diameter hose was preferred rather than clusters of smaller diameter conduits, as this simplified the entire filling procedure and made the system more manageable. Normal plastic hose was chosen as it is readily available and affordable for testing purposes. Brass gas line fittings and valves were used to prevent air being sucked into the system. The system consists of a water source which is placed below the “leaf”, a ball valve (V-1) to shut off flow from the water source and a needle valve (V-2) that is connected to a small laboratory ejector vacuum pump which is used to remove air and

accumulated bubbles. The winglets (13), shown in Figure 9, are used to secure the “leaf” to a frame or supporting structure.

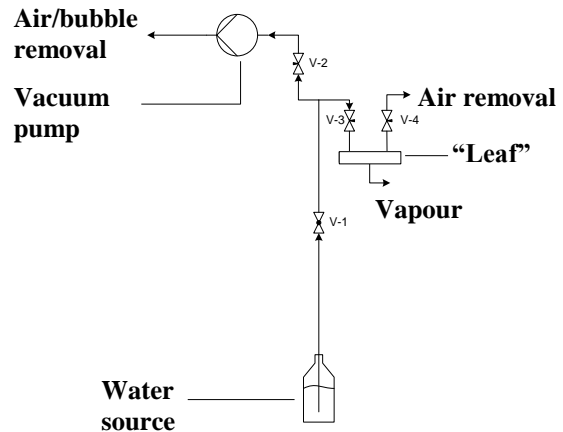


Figure 12: Flow diagram of a single “leaf” water pump

Two multiple “leaf” system were also constructed. One featured a single water source and the other featured independent water sources for each “leaf”. The “leaf” layout is shown in Figure 13, where each “leaf” was attached to a large 8 mm thick perspex sheet. Two axial flow fans were attached before leaves 3 and 9.

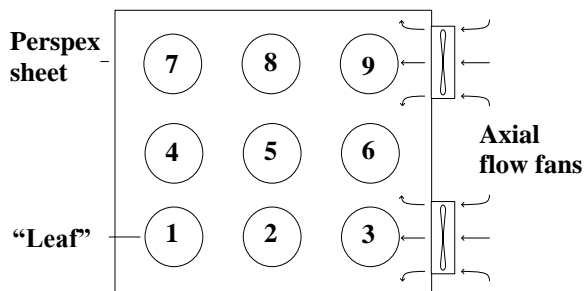


Figure 13: Multiple “leaf” layout

*Theoretical Modelling:* Modelling of the STDWP for various environmental conditions was done. Considering a simple flow resistance diagram of a single “leaf” branch, as shown in Figure 14, it can be seen that the amount of water evaporated from the “leaf” would be the same amount that leaves the water source if no water is being added or extracted from the system.

It was further assumed that the entire surface area of the evaporative layer is fully wetted at all times. This assumption was made as the surface of the MF-Millipore™ filter is highly irregular, as seen in Figure 11 (d), and the number of pores is not known. Therefore, simple mass transfer equations may be used to model the evaporative rate from the “leaf”. The following equations on mass transfer were sourced from Çengel et al. [32]. The general mass transfer

equation can be written as

$$\dot{m}_v = h_{mass} A_s (\rho_{v,s} - \rho_{v,\infty}) \quad (7)$$

where  $\dot{m}_v$  is the evaporation rate,  $h_{mass}$  is the convective mass transfer coefficient,  $A_s$  is the exposed surface area,  $\rho_{v,s}$  is the density of the vapour near the evaporative surface and  $\rho_{v,\infty}$  is the vapour density far away from the surface.  $h_{mass}$  is defined as

$$h_{mass} = \frac{Sh D_{AB}}{L_c} \quad (8)$$

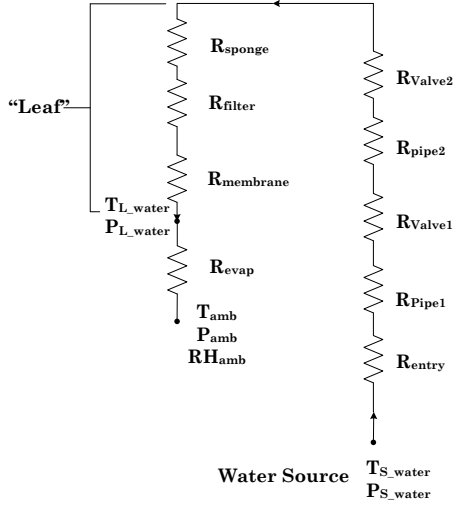


**Figure 14: Simple flow resistance diagram of a single “leaf” branch**

where  $Sh$  is the dimensionless Sherwood number,  $D_{AB}$  is the mass diffusivity of species  $A$  in  $B$  and  $L_c$  is a characteristic length. The  $Sh$  number relations for a horizontal plate facing downward are shown in Table 2.

**Table 2: Sherwood number formulations for forced and natural convection over a downward facing horizontal plate [32]**

Region		Sherwood number
Forced Laminar	$Re < 5(10)^5$ $Sc > 0.5$	$0.664 Re_L^{0.5} Sc^{1/3}$
Forced Turbulent	$5(10)^5 < Re < 10^7$ $Sc > 0.5$	$0.037 Re_L^{0.8} Sc^{1/3}$
Natural	$10^5 < Gr Sc < 10^{11}$ $\rho_s < \rho_\infty$	$0.27 (Gr Sc)^{1/4}$

where  $Re$  is the Reynolds number,  $Sc$  is the Schimdt number, and  $Gr$  is the Grashof number which are defined respectively as

$$Re = \frac{v_f L_c}{\nu} \quad (9)$$

$$Sc = \frac{\nu}{D_{AB}} \quad (10)$$

$$Gr = \frac{g(\rho_\infty - \rho_s)L_c^3}{\rho\nu^2} \quad (11)$$

where  $v_f$  is the fluid velocity and  $\nu$  is the fluid kinematic viscosity ( $\frac{\mu}{\rho}$ ). For fluid flow in the branch tubing driven by evaporation, it can be assumed that the flow will be rather slow and laminar. It can easily be shown from basic momentum and mass conservation that the pressure drop over a vertical pipe section is

$$\Delta P = \frac{8\mu\Delta x\dot{V}}{\pi r_s^4} + \rho gh \quad (12)$$

where,  $\dot{V}$  is the volume flow rate,  $\Delta x$  is the pipe length,  $r_s$  is the pipe radius and  $h$  is the vertical pipe length. Due to the very slow flow rates expected, it can be shown that pressure losses due to the valves, fittings and entry effects are negligible. For these low flow rates, Darcy’s law, Equation 13, for flow through porous materials is assumed to be valid for flow through the internal “leaf” material [33]. The pressure drop over the internal “leaf” material may then be approximated as

$$\Delta P = \frac{\mu\Delta x}{\kappa A_c} \dot{V} \quad (13)$$

where,  $\kappa$  is the porous material’s intrinsic permeability and  $A_c$  is the cross-sectional area of the porous material.  $\kappa$  is an empirical term which is generally acquired through experimentation with porous materials. Further, as the pipe diameter is relatively large and the flow rate quite small, it is safe to assume that the pipe flow resistance will be insignificant when compared to the pressure head. Additionally, the flow resistance due to the porous material should be accounted for, however, at very high pumping heads this too will be rather small due to the extremely slow volume flow rates expected.

**Experimentation:** Various experiments were conducted to determine the STDWP’s behaviour and performance under various conditions. Initial tests were conducted with the single “leaf” system and the multiple “leaf” system. A schematic of the test setup for a single “leaf” shown in Figure 15. For the tests, the “leaf” (1) was fixed to a supporting frame (2), approximately 1 m to 1.8 m above the water source (3), after the initial filling was completed. These tests further required an axial flow fan (4) to force air flow over the “leaf”. Humidity sensors were used to measure the ambient air temperature and relative humidity at the evaporative surface of the “leaf”. Additionally, the *RS232 BTU-PSYCHROMETER AZ 8912* with a built in anemometer was used to measure the average air velocity over the each “leaf” surface. Red die was added to the water source to monitor the water movement up the branch tubing (5) over time.

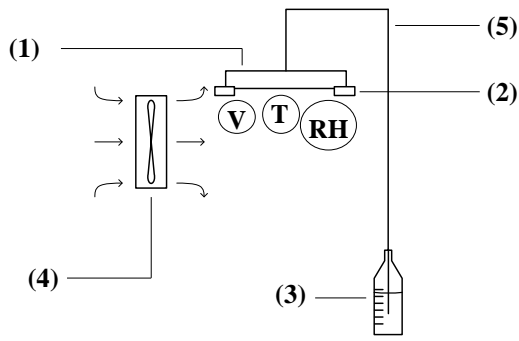


**Figure 15: Schematic of single “leaf” test setup**

The multiple “leaf” layout is shown in Figure 13 while the actual multiple “leaf” test is shown in Figure 16 (a). The “leaves” were fixed to a wooden frame (1) approximately 1.5 m above the ground. Axial flow fans (1) were placed at “leaves” numbered 3 and 9. The independent water sources (3) used for the multiple “leaf” tests are shown in Figure 16 (b).

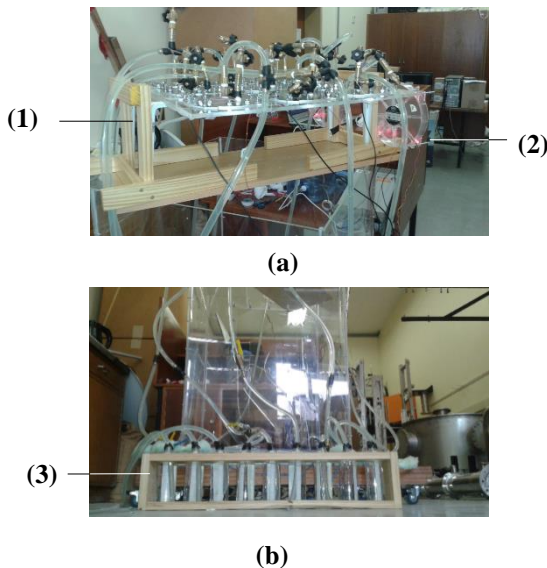


**Figure 16: (a) Multiple “leaf” testing with (b) multiple water sources for each “leaf”**

The initial water level was marked and after a certain time interval the new water level was recorded. The volume change of water in the water source over time was used to estimate the volumetric flow for each measurement interval. Much care was taken to ensure that an accurate recording of the time and water level was made for each measurement. For the multiple “leaf” tests the air velocity and environmental conditions were monitored at the various “leaf” surfaces. The multiple “leaf” tests, where a single water source was used, required a distribution manifold. During testing it was found that the manifold system presented much difficulty as trapped air and leaks were detrimental. Further, if a single branch failure occurred the entire system would be corrupted.

Therefore, the multiple “leaf” system with separate water sources for each “leaf” was used to determine the behaviour of grouped “leaves”.

To determine the potential pumping head of the STDWP, the “leaf” was taken to progressively higher heights, as shown in Figure 17, until a failure occurred either due the capillary limit or cavitation in the pipes. Finally, the water collection capability for a single “leaf” was tested, as shown in Figure 18. Here, a single “leaf” (1) was placed in an environmental control chamber (2).

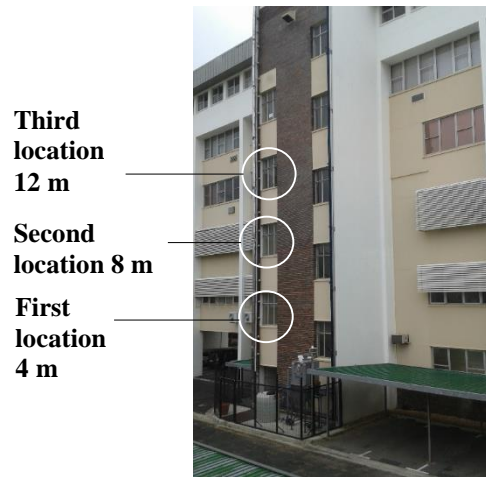


**Figure 17: Potential water pumping head test locations**

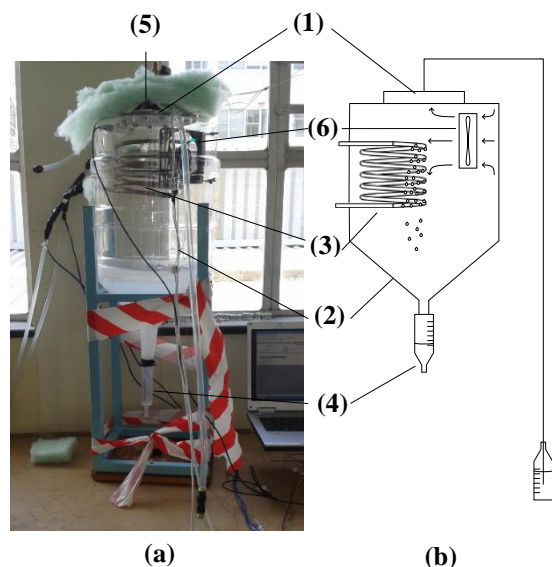


**Figure 18: (a) Water collection testing with a (b) schematic of the test**

Inside the control chamber copper cooling coils (3) were used to condense the evaporated water from the “leaf”. A collection container (4) inside the control chamber was used to collect the condensate. To increase evaporative rates, a 9 W heating pad (5) was placed on top of the “leaf” and insulated. Further, an



axial flow fan (6) was placed inside the chamber to force air flow over the surface of the “leaf” and to promote air circulation. Temperature and humidity sensors and the AZ8912 was once again used to measure the control chambers environmental conditions ( $v_{air}$ ,  $T_{leaf}$ ,  $T_{amb}$  and  $RH_{amb}$ ).

**Results and Discussion:** The captured experimental data from the aforementioned tests was manipulated to report on the STDWP’s pumping performance, functional lifespan and general behaviour at various environmental conditions ( $v_{air}$ ,  $T_{leaf}$ ,  $T_{amb}$  and  $RH_{amb}$ ). In general the tests were separated into a forced and natural convection case. A statistical multi-linear regression was applied to the single “leaf” data for the single “leaf” testing and statistical predictions were then made for the same conditions. Using the recorded environmental conditions together with the theoretical mass transfer relations discussed earlier, theoretical predictions were also made. Figure 19 shows a comparison of the theoretical as well as statistical predictions compared to the experimental results.

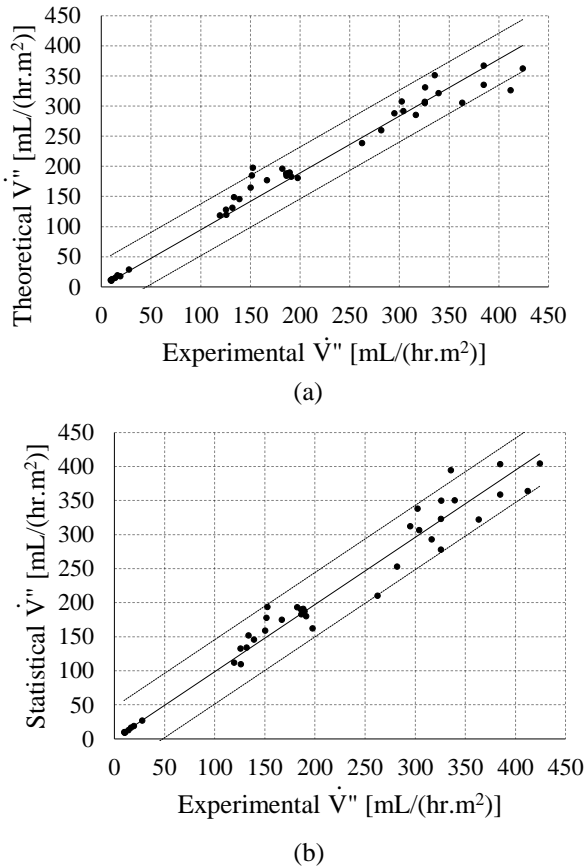


**Figure 19: (a) Theoretical and (b) statistical evaporative flux predictions compared to experimental results.**

A power series of the following form was assumed to describe the evaporative flux data.

$$\dot{V}'' = av_{air}^{b1} T_{leaf}^{b2} T_{amb}^{b3} RH_{amb}^{b4} \quad (14)$$

After manipulation, the above power series becomes

$$\ln(\dot{V}'') = \ln a + b_1 \ln v_{air} + b_2 \ln T_{leaf} + b_3 \ln T_{amb} + b_4 \ln RH_{amb} \quad (15)$$

Statistical multi-linear regression was then applied to the manipulated data by using Equation 15. For the statistical analysis a maximum and average residual error of 8.4% and 27.49% was observed, respectively. Figure 19 (b) shows a comparison of the statistical (forced and natural convection) evaporative flux predictions with the experimental results. Here a good correlation between the statistical formulations and experimental data is shown. An overall R<sup>2</sup> of 96.5% and an error margin of 47.32 mL/hr.m<sup>2</sup> at a 95% confidence level was obtained. The theoretical predictions achieved a maximum residual error of 30.26% and an average residual error of 7.41%, respectively. Figure 19 (a) shows the theoretical (forced and natural convection) evaporative flux predictions compared to the experimental results. The theoretical results displays a good correlation to the experimental measurements as an overall R<sup>2</sup> of 96.6% and an error margin of 42.93 mL/hr.m<sup>2</sup> at a 95% confidence level was acquired

A sensitivity analysis was also conducted which showed that the simplified statistical formulations performed poorly under extrapolation. Here the environmental conditions were varied from a specific base condition to determine to which degree these environmental factors affect the evaporative flux. Therefore, the theoretical predictions, calculated with mass transfer relations, were found to be more accurate over a larger range of conditions and used in all further calculations. The addition of heat to the “leaf” surface was tested with the 9 W heating pads allowing “leaf” water temperatures of 35 °C to be reached. With an increase in the water temperature large increases in evaporative rates were observed. The addition of heat, however, required the use of de-aerated water as well as a gasket between the lower disk and membrane filter see (9) in Figure 9.

The multiple “leaf” testing has a “leaf” layout as shown in Figure 13. Two axial flow fans were attached before “leaves” numbered 9 and 3. During the multiple “leaf” testing it was found that the use of a manifold to connect the various branches allowed for multiple branch corruption due to a single branch failure. Further, the initial filling procedure was unnecessarily complicated by trapped air in the manifold. Therefore, the only useful results were obtained during the multiple “leaf” tests employing separate water sources for each “leaf”. Table 3 summarises the theoretical error obtained for each row of leaves. Row 1 contains “leaves” numbered 3, 6 and 9; where row 2 contains “leaves” 2, 5 and 8; and finally row 3 contains “leaves” numbered 1, 4 and 7.

From Table 3 it is clear that the theoretical error increases with each row further away from the axial

flow fans. It was observed that the “leaves” closest to the axial flow fans displayed more predictable behaviour as with the single “leaf” tests. However, “leaves” further away from the axial flow fans were found to display far less predictable behaviour. This discrepancy where the theoretical results far overestimate the actual “leaf” performance were attributed primarily to humid boundary layers, stagnant zones and inconsistent cross flows due to flow turbulence. A discrepancy in nature is often also observed as single leaf transpiration rates observed do not scale correctly when compared to the entire canopy transpiration rate observed [34].

**Table 3: Theoretical prediction error from experimentally measured evaporation rate results for multiple “leaf” testing**

Row	Max error %	Ave error %	Min error %
1	16.12	7.09	3.96
2	39.47	23.95	14.54
3	63.65	43.00	15.57

The single “leaf” tests were conducted at various heights to estimate the effect of pumping head on the STDWP’s water pumping performance. Heights up to nearly 6 m were monitored. It was found, for the pumping heads tested here, that the evaporation rate from the “leaf” surface consistently remained the same (theoretical estimates) irrelevant of the pumping head. For low pumping heads it is believed that the evaporation rate will remain fairly similar for the same environmental conditions. However, as the pumping head is increased to much higher pumping heads, the evaporation rate from the surface of the “leaf” might decrease somewhat. Considering much higher pumping heads it is clear, from Equation 12, that as  $h$  increases the pressure drop over the system will increase. Consequently, from Equation 2, a more negative Laplace pressure will be observed and therefore a larger interfacial curvature. A more receded meniscus will result and therefore the interface will be further removed from the environment. Additionally, Equation 5, indicates that an increased interfacial curvature will result in a lowered vapour pressure. Both a receded meniscus and lowered vapour pressure will result in a lowered evaporation rate. The degree at which the evaporation rate will decrease is primarily related to the pumping head, number of pores and pore geometry. As shown in Figure 11, the membrane filter used has a highly irregular surface and the number of pores and their actual sizes are not known. Therefore, the extent of the reduction in evaporation rate is difficult to estimate. Subsequently, for the theoretical analysis of the various tests it was assumed that the membrane was fully wetted at all times and height was neglected after determining the evaporative flux.

Although the pumping head had little effect on the evaporation rate from the “leaf”, the pumping head height, however, was found to greatly affect the pump’s functional lifespan. Figure 20 shows the time to failure as the pumping head is increased.

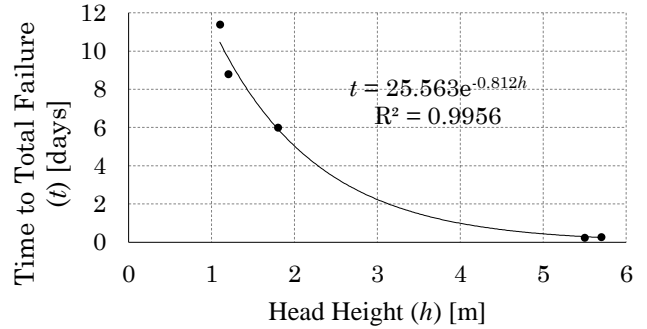


**Figure 20: Water pumping head effect on pump functional lifespan**

For pumping heads of roughly 1 to 1.8 m the functional lifespan of the STDWP was 6 to 13 days. Higher heights from 5 to 6 m resulted in complete failure within a few hours. It was initially believed that gradual bubble collection resulted in the premature system failure. However, the pump failure still occurred in roughly the same time even after deaerating the test water and with the absence of observable bubbles in the branch tubing. The failure is not believed to be due to the capillary limit being exceeded as the membrane filter has a bubble pressure rating of approximately 3.5 bar [30] (which is far above the required interfacial pressures at which the tests operate). This is further supported by noting that the system failure was not instantaneous, as would be the case if the capillary limit was exceeded. The rather short functional lifespan of the STDWP is suspected to be a result of gradual membrane damage over time due to the strong interfacial forces. Considering a simple force diagram of a capillary tube as shown in Figure 21, it is can be seen that the surface tension force ( $F_\sigma$ ) is both pulling the liquid upward and pulling inward on the capillary walls. The magnitude of  $F_\sigma$  is directly related to the pumping head, as the required Laplace pressure increases with height. The membrane filter under normal use is not exposed to an air-water interface with such large interfacial pressures and surface tension forces. The bubble pressure tests, conducted on such membrane filters, do not indicate nor imply that the membrane filters are able to sustain large interfacial forces for prolonged periods of time. The bubble pressure tests is simply used as a means to determine the largest effective capillary radius for the membrane filter. Therefore, surface tensions forces are suspected to be the mechanism that eventually affects the pore integrity as well as eventually damages the membrane filter. This might explain why the STDWP’s functional lifespan is height related. Both Susman et al. [4] and Martinez Vilalta et al. [5] found

that their artificial trees failed in roughly the same amount of time and that the failure was attributed to membrane damage.

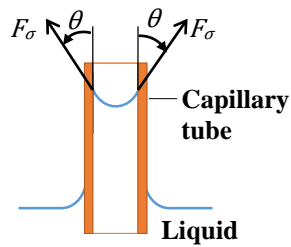


**Figure 21: Force diagram of a simple capillary tube**

The highest pumping head which should be theoretically obtainable with respect to the membrane specifications is nearly 30 m. The actual highest pumping head obtained was approximately 10.1 m, which is much lower than the estimated maximum height. For the maximum potential pumping head tests, as shown in Figure 17, de-aerated water was used. At heights, near 8 m it was observed that the water still contained some residual air as tiny bubbles formed in the branch tubing. The residual air and tiny bubbles were removed before higher head heights were attempted. At 9.8 m of head height some of the remaining tiny air bubbles coalesced into a single large bubble. The system, however, did not fail at this height. As the maximum pumping head was reached, spontaneous and erratic bubble formation occurred throughout the highest branch sections. The water level then dropped to roughly 9.8 m. For the test conditions, water vaporisation in the branch tubes was estimated to occur at roughly 9.85 m. Therefore, water was indeed in a metastable state when the highest pumping head was reached. It is believed that the plastic tubes (which are hydrophobic) provided poor adhesive forces and heterogeneous nucleation occurred in the branch tubing. For a non-wetting material, such as the PVC plastic tubing used, the formation of air pockets which provide nucleation sites for heterogeneous nucleation is much greater than for a wetting material<sup>20</sup>. A capillary failure is not suspected as the pressure head is far below the bubble pressure specification for the membrane filter. Further, the water was under a slight tension when the water column broke. Additionally, the water column did not fall all the way down to the ground, but stabilised near the saturated vaporisation threshold and therefore a vacuum must still be present on the “leaf” side. In the case of a capillary failure, tiny bubble would continually stream into the system until all the water has receded to the ground.

During the water collection testing the environmental control chamber had stabilised internal temperatures ranging from 12 to 13 °C where the internal humidity varied between 75 to 80%. “Leaf” temperatures of 14 to 15 °C were measured. This allowed average evaporation rates of approximately 1.57 mL/hr to be

obtained. Furthermore, the collected water was on average 98% of the water measured leaving the water source. At times the water collection percentage varied with  $\pm 10\%$  as some residual water remained on the cooling coils when the measurement was made.

Certain factors were identified to add to experimental error. For the volumetric flow calculation water level marks were made on the water source at certain time intervals. Great effort went into ensuring accurate markings were made and the meniscus as well as marker thickness accounted for. A double measurement using a fine syringe as well as a laboratory measuring flask was done to reaffirm the measurement. This process of measuring was found to produce possible complications as residual water content and parallax errors were difficult to avoid. Furthermore, bubble growth in the branch tubing increased errors. Figure 22 shows an image of small bubbles and a large bubble found in the tubing.



**Figure 22: (a) Small and (b) large bubble formation in branch tubing**

Tiny bubbles were found to have a negligible effect on the water height measurement, however, when bubbles grew substantially larger a certain volume of water would be forced back down to the water source. Therefore, the de-aeration of water was crucial as bubble accumulation would skew the water level measurement over time.

For the theoretical analysis of the measured data, all environmental conditions were averaged between the measurement intervals. This was done to determine the predictability of a “leaf” given a constant design criteria. During certain days, especially rainy days where intermittent showers and sunny conditions persisted, many temperature, relative humidity and pressure variations prevailed. Unpredictable weather patterns therefore influenced the averaging process. It was also noticed that for shorter measurement intervals greater evaporative rate variations were observed. For longer measurement intervals, on the other hand, more stable evaporative rates were obtained, as expected.

Figure 23 shows a used PVA sponge stained with red dye. Here it can be seen that the surface wetting is not complete, nor is it equal in all directions. The assumption that the entire surface area of the membrane is fully wetted at all times may therefore be questioned. This may also present some error in the theoretical analysis.



**Figure 23: Red die stains on PVA Sponge**

Instrumental error was deemed to play a minor role in experimental error as the thermocouples and data loggers were all calibrated and found to have an error less than  $\pm 0.5$  °C. The axial flow fans used also produced a stable flow rate with minor variations. The natural convection case was found to be very susceptible to instrumental error as small temperature changes significantly affected the predicted evaporative rate.

The surface tension driven pump developed was able to pump water primarily through a combination of evaporation and surface tension. The functional lifespan of the pump was, however, found to be very short and the regular replacement of membrane filters and system refilling to be a tedious and costly process with minimal gain. It is therefore recommended that the evaporative surface be constructed of a much more rigid/reinforced material that is able to sustain the large interfacial forces as result of surface tension. In an effort to closer replicate the plant vascular system as well as to better utilise the adhesive properties of water, clusters of smaller diameter tubing which consists of a high surface energy material is also recommended to achieve higher pumping heads. For a system where a distribution manifold is desired, the development of pit-like structures is required to remove the need for constant system monitoring and avoid multiple branch corruption. The use of membrane filters, as used in the “leaf”, will replicate pit-membranes found in plants. The number of artificial pits must be limited as the flow resistance will increase and result in a large capillary limit requirement for the evaporative surface. The deactivation of gas filled micro cavities in the branch tubing must also be attempted if higher pumping heads are desired. Further, multiple flow entry points into the “leaf” is recommended as this will promote even spreading of water onto the membrane filter which will prevent localised membrane drying and damage. Finally, stomatal control may be attempted [35] as to provide a more stable flow rate and impede bubble formation at higher pumping heads.

**Conclusion:** In conclusion, the developed STDWP was determined to be a potential water pump. Although the flow rates are slow the pumping requires no electricity input. The pump however still requires much development as the functional lifespan must be increased to create a more viable pump alternative. It

is therefore recommended that an alternative more rigid/reinforced evaporative surface material as well as the use of clustered smaller diameter tubing of a highly hydrophilic material be considered to improve the pump’s functional lifespan and pumping head height.

#### References:

1. IBTimes. 2012. Biomimicry: *Designing the Future with Mother Nature's Help* [Online]. Available: [http://au.ibtimes.com/articles/252878/20111121/biomimicry-designing-future-mother-nature-s-help\\_\\_4.htm](http://au.ibtimes.com/articles/252878/20111121/biomimicry-designing-future-mother-nature-s-help__4.htm) [Accessed 24 July 2013].
2. Leybovich, I. 2012. *Mother Nature as Muse: The Future of Design* [Online]. Industry Market Trends. Available: <http://news.thomasnet.com/IMT/2012/04/10/mother-nature-as-muse-the-future-of-design/> [Accessed 29 July 2013].
3. Koch, K. and Barthlott, W. 2009. Superhydrophobic and superhydrophilic plant surfaces: an inspiration for biomimetic materials. *Philosophical Transactions of the Royal Society A: Mathematical, Physical and Engineering Sciences*, 367(1893), 1487-1509.
4. Susman, K., Razpet, N., et al. 2009. *Modeling The Water Transport In Tall Trees*. Faculty of Education, University of Ljubljana, Slovenia.
5. Martinez Vilalta, J., Sauret, M., et al. 2003. Make your own transpiring tree. *Journal of Biological Education*, 38(1), 32-35.
6. Namasivayam, V., Larson, R. G., et al. 2003. Transpiration-based micropump for delivering continuous ultra-low flow rates. *Journal of Micromechanics and Microengineering*, 13(2), 261-271.
7. Wheeler, T. D. and Stroock, A. D. 2008. The transpiration of water at negative pressures in a synthetic tree. *Nature*, 455(7210), 208-212.
8. Berry, S. and Kedzierski, J. 2008. New Methods to Transport Fluids in Micro-Sized Devices. *Lincoln Laboratory Journal*, 17(2).
9. Borno, R. T., Steinmeyer, J. D., et al. 2009. Charge-pumping in a synthetic leaf for harvesting energy from evaporation-driven flows. *Applied Physics Letters*, 95(1).
10. Reece, S. Y., Hamel, J. A., et al. 2011. Wireless Solar Water Splitting Using Silicon-Based Semiconductors and Earth-Abundant Catalysts. *Science*, 334(6056), 645-648.
11. Biello, D. 2013. 400 PPM: *Can Artificial Trees Help Pull CO2 from the Air?* Available: <http://www.scientificamerican.com/article/prospects-for-direct-air-capture-of-carbon-dioxide/> [Accessed 06 June 2014].
12. Banks, M. 2009. *Engineers call for 'artificial trees' to reduce CO2*. Available: <http://physicsworld.com/cws/article/news/2009/aug/27/engineers-call-for-artificial-trees-to-reduce-carbon-dioxide> [Accessed 06 June 2014].
13. Sang Kug, C., Kyungjoo, R., et al. A Surface-Tension-Driven Propulsion and Rotation Principle for

- Water-Floating Mini/Micro Robots. Micro Electro Mechanical Systems, 2009. MEMS 2009. *IEEE 22nd International Conference on*, 25-29 Jan. 2009 2009. 1083-1086.
14. Angelini, T. E., Roper, M., et al. 2009. Bacillus subtilis spreads by surfing on waves of surfactant. *Proceedings of the National Academy of Sciences*, 106(43), 18109-18113.
15. Carey, V. P. 1992. *Liquid-vapor Phase-change Phenomena: An Introduction to the Thermophysics of Vaporization and Condensation Processes in Heat Transfer Equipment*. 1 ed.: Hemisphere Publishing Corporation.
16. Israelachvili, J. N. 2011. *Intermolecular and Surface Forces*: Revised Third Edition, Elsevier Science.
17. Butt, H. J. and Kappl, M. 2009. *Surface and Interfacial Forces*. Weinheim: Wiley.
18. Coder, K. D. 1999. *Basic Water Properties: Attributes and Reactions Essential for Tree Life*. The University of Georgia.
19. Peramaki, M. 2005. *A physical analysis of sap flow dynamics in trees*. Department of Forest Ecology, University of Helsinki.
20. Carey, V. P. 2008. *Liquid-vapor Phase-change Phenomena: An Introduction to the Thermophysics of Vaporization and Condensation Processes in Heat Transfer Equipment*. 2 ed.: Taylor & Francis Group, LLC.
21. Caupin, F., Arvengas, A., et al. 2012. Exploring water and other liquids at negative pressure. *Journal of Physics: Condensed Matter*, 24(28), 284110.
22. Davitt, K., Rolley, E., et al. 2010. Equation of state of water under negative pressure. *The Journal of Chemical Physics*, 133(17).
23. Sedgewick, S. A. and Trevena, D. H. 1976. Limiting negative pressure of water under dynamic stressing. *Journal of Physics D: Applied Physics*, 9(14), 1983.
24. Starr, C., Taggart, R., et al. 1978. *Biology: The Unity and Diversity of Life*. 4 ed. Belmont: Wadsworth.
25. Campbell, N. A. and Reece, J. B. 2008. *Biology*. 8 th ed. Boston: Benjamin Cummings: Pearson.
26. Nichols, M. 2014. *Redwoods: The Super Trees* [Online]. Available: <http://ngm.nationalgeographic.com/2009/10/redwoods/nichols-photography#/04-lone-tree-714.jpg> [Accessed 15 March 2014].
27. Sperry, J. S. 2011. *Hydraulics of vascular water transport*. Signaling and Communication in Plants: Mechanical Integration of Plant Cells and Plants. Berlin: Springer.
28. Choat, B., Cobb, A. R., et al. 2008. Structure and function of bordered pits: new discoveries and impacts on whole-plant hydraulic function. *New Phytologist*, 177(3), 608-626.
29. BBC. 2013. *Photosynthesis* [Online]. Available: [http://www.bbc.co.uk/schools/gcsebitesize/science/ad\\_d\\_edexcel/organism\\_energy/photosynthesisrev1.shtml](http://www.bbc.co.uk/schools/gcsebitesize/science/ad_d_edexcel/organism_energy/photosynthesisrev1.shtml) [Accessed 18 February 2014].
30. Merck Millipore. 2014a. *MF-Millipore™ Membrane Filters*. [Online]. Available: [http://www.emdmillipore.com/GB/en/product/MF-Millipore%E2%84%A2-Membrane-Filters,MM\\_NF-C152](http://www.emdmillipore.com/GB/en/product/MF-Millipore%E2%84%A2-Membrane-Filters,MM_NF-C152). [Accessed 26 September 2014].
31. Merck Millipore. 2014b. *Durapore® Membrane Filters*. [Online]. Available: [http://www.emdmillipore.com/US/en/product/Durapore%C2%AE-Membrane-Filters,MM\\_NF-C7631](http://www.emdmillipore.com/US/en/product/Durapore%C2%AE-Membrane-Filters,MM_NF-C7631). [Accessed 26 September 2014].
32. Çengel, Y. A., Ghajar, A. J., et al. 2011. *Heat and Mass Transfer: Fundamentals and Applications*. 4 ed. New York: McGraw Hill Higher Education.
33. Truskey, G. A., Yuan, F. & Katz, D. F. 2010. *Transport Phenomena in Biological Systems*, Pearson Prentice Hall.
34. Meinzer, F. C. 1993. Stomatal control of transpiration. *Trends in Ecology & Evolution*, 8(8), 289-294.
35. Wessels, F. J. 2013. *Biomimetic Surface Area Control Mechanism*. Final Year Engineering Project. University of Stellenbosch: Department of Mechanical and Mechatronic Engineering.